A numerical study of aerosol effects on the dynamics and microphysics of a deep convective cloud in a continental environment

Zhiqiang Cui,[1] Kenneth S. Carslaw,[1] Yan Yin,[2] and Stewart Davies[1]

Received 16 March 2005; revised 1 November 2005; accepted 17 November 2005; published 1 March 2006.

[1] The effects of aerosols on a deep convective cloud in a midlatitude continental environment are studied using an axisymmetric cloud model with a sectional treatment of aerosol and hydrometeor microphysical processes. Simulations are conducted using observations from the Cooperative Convective Precipitation Experiments (CCOPE). The isolated cloud occurred in an environment with low wind shear and with relatively dry air in the midtroposphere and upper troposphere. By varying the concentration of aerosol particles in the accumulation mode within realistic limits for a continental environment, the simulated cloud exhibited different properties. The overall impact as the aerosol concentration increased is that (1) the cloud development was inhibited; (2) the precipitation was suppressed; (3) the maximum values of liquid water content decreased, but the maximum values of droplet number concentration increased before the dissipating stage; (4) a clear tendency was found for ice crystals to be larger and less numerous in the anvil cloud; and (5) there was a significant reduction of the inflow in the lower 2 km of the atmosphere. In the relatively dry environment in the midtroposphere, the latent heat changes associated with the Wegener-Bergeron-Findeisen mechanism played an important role in the upper part of the cloud at altitudes below the homogeneous freezing level. In particular, immersion freezing and latent heat release were much more rapid in the base simulation than in the increased aerosol simulation. Less latent heat release and insufficient inflow together impeded the development of the cloud with the higher aerosol loading. Our simulations suggest that continental clouds existing below the homogeneous freezing level could show an opposite response of cloud top height and anvil crystal concentrations to changes in aerosol to what has previously been reported for clouds ascending to higher levels.

Citation: Cui, Z., K. S. Carslaw, Y. Yin, and S. Davies (2006), A numerical study of aerosol effects on the dynamics and microphysics of a deep convective cloud in a continental environment, *J. Geophys. Res.*, *111*, D05201, doi:10.1029/2005JD005981.

1. Introduction

[2] Atmospheric aerosols can be very effective cloud condensation nuclei (CCN) and therefore have the potential to influence cloud microphysical processes and rainfall production efficiencies. Aerosols affect not only clouds but also regional and global climate changes. They influence the radiative budget of the Earth directly by the modulation of atmospheric scattering [*Charlson et al.*, 1992] and absorbing [*Ramanathan and Vogelmann*, 1997] properties and indirectly by the modification of cloud albedo [*Twomey*, 1991], lifetime [*Albrecht*, 1989], precipitation [*Rosenfeld*, 2000] and extent [*Ramanathan et al.*, 2001]. Atmospheric aerosols are currently one of the largest sources of uncertainty in quantifying global and regional climate change [*Intergovernmental Panel on Climate Change* (*IPCC*), 2001]. The influence of aerosols on cloud properties and hence the influence on the hydrological cycle and the indirect effect on climate are key challenges because many chemical and microphysical properties/processes of aerosol that affect clouds are not well understood.

[3] Deep convective clouds are especially important for the transfer of water substance, trace gases and aerosols to the upper troposphere. They influence latent heating that warms the atmosphere and drives major circulation features of the atmosphere. They also produce extensive anvils in the upper troposphere. The study of the effect of aerosols on convective clouds will not only help to improve our understanding of precipitation development but will also improve our understanding of their effect on the climate [*Graf*, 2004].

[4] Observations of deep mixed-phase convective cloud response to aerosols are very limited. The recent observations over Amazonia [*Andreae et al.*, 2003] revealed that high aerosol abundances from smoke suppress low-level rain production, thereby allowing transport of liquid water to upper levels. The increase of the altitude of precipitation generation invigorates the updrafts and causes intense thunderstorms. Other observations have focused on shal-

[1] Institute for Atmospheric Science, School of Earth and Environment, University of Leeds, Leeds, UK.
[2] Department of Applied Meteorology, Nanjing University of Information Science and Technology, Nanjing, China.

0148-0227/06/2005JD005981$09.00

lower clouds [*Rosenfeld and Woodley*, 2000; *Rosenfeld*, 2000] or have studied clouds in only a single aerosol environment [*Rosenfeld and Woodley*, 2000].

[5] Numerical models of cloud microphysics and dynamics are essential tools for investigating the mechanisms by which aerosols influence cloud microphysics and dynamics. Models are also essential for exploring environmental and aerosol conditions where cloud responses may not be so easily observed as over Amazonia. Only a limited number of studies have used numerical models to examine the impact of aerosols on mixed phase convective cloud microphysics and dynamics in different environments. Some studies have focused on the microphysical changes resulting from changes in the aerosol without examining the dynamical responses of the cloud [e.g., *Phillips et al.*, 2002; *Ekman et al.*, 2004]. *Khain et al.* [1999] studied the response of Mediterranean mixed phase clouds to varying aerosol concentrations typical of maritime and continental humid conditions. They found that the rate of warm rain formation can be several times lower when aerosol concentrations are high and that the increased droplet concentrations above the freezing level produce a large number of small graupel particles and ice crystals. *Fridlind et al.* [2004] used a combination of field observations and detailed cloud microphysics simulations to show that the entrainment of midtropospheric aerosols can dominate the number of ice crystals in the anvils of deep subtropical clouds. *Khain et al.* [2004] developed a spectral microphysics mixed-phase cumulus cloud model and applied the model to deep cumulus clouds occurring in Texas [*Rosenfeld and Woodley*, 2000]. In their simulations, the aerosol concentration was 1260 cm^{-3} for what they termed a "continental case" and 100 cm^{-3} for a "maritime case." They found a significant decease in accumulated precipitation when aerosol concentrations were high and showed that increased aerosol concentrations result in a higher number of smaller crystals at cloud top. This result is in agreement with *Fridlind et al.* [2004] and can be explained in terms of the number of droplets ascending above the homogeneous freezing level. *Khain et al.* [2004] also showed that varying the aerosol concentration significantly influenced cloud dynamics, with the clouds being deeper and more vigorous when aerosol concentrations were high. In the *Phillips et al.* [2002] study of a cloud over New Mexico, they also found that in the deep phase of cloud development (up to $\sim$9 km) the number of crystals in the anvil increased with aerosol concentration beyond typical continental values. *Yin et al.* [2000] have also studied the effect of giant nuclei on cloud microphysics and found that the coalescence between water drops was enhanced, resulting in the earlier development of large drops in the lower levels of the clouds. It is found that the ice phase process is dependent on aerosols, though the nucleation process can proceed via different pathways and from a variety of different nucleating chemical species [*IPCC*, 2001].

[6] Many of these studies have focused on very deep convection ascending above the homogeneous freezing level of around $-40°C$. However, mixed phase convective clouds with a vertical extent and cloud top temperature at or below the homogeneous freezing level, such as studied in this paper, have received relatively little attention.

[7] Recently *Yin et al.* [2005] conducted a modeling study of vertical transport and processing of sulphate aerosol by a moderately deep mixed-phase convective cloud in a continental environment, and examined the feedback of the cloud-processed aerosols on the development of cloud microphysical properties and precipitation. In that study we found that the increased abundance of cloud condensation nuclei caused by reentrainment of processed aerosol at midlevels led to a decrease in crystal concentration at cloud top around 10 km, an opposite response to that simulated in the other studies reported above.

[8] In this paper, simulations are conducted using an axisymmetric nonhydrostatic numerical model of the same convective cloud as studied by *Yin et al.* [2005]. The purpose is to numerically study the effects of aerosol on the dynamics and microphysics of a deep convective cloud in a continental environment which is well characterized by observed meteorological conditions [*Yin et al.*, 2005]. The focus will be on the processes that cause the changes in the microphysics and dynamics due to the changing aerosol size distributions.

[9] The structure of the paper is as follows. The numerical model is briefly described first. We then describe the experimental design, which includes the variations of the size distributions of aerosol and the humidity. In the results section, we describe the effects of the various initial aerosol size distributions on the cloud microphysics and dynamics. Finally, we compare our results with similar previous studies.

2. Numerical Model

[10] The numerical model for this study is the Model of Aerosols and Chemistry in Convective Clouds (MAC3). The model dynamics and microphysics are based on the axisymmetric nonhydrostatic cloud model of *Reisin et al.* [1996]; trace gas and aerosol modules are newly added features and are described fully by *Yin et al.* [2002] and *Yin et al.* [2005]. Only a brief description is given here.

[11] The governing equations include the following atmospheric variables: the vertical and radial velocity, the pressure perturbation, the virtual potential temperature perturbation, the specific humidity perturbation, the specific number concentration and mass of aerosol in a spectral bin, the specific number concentration and mass for each type of cloud particle in a size bin, and the concentration of activated ice nuclei. The microphysical processes are solved with an accurate multimoment method [*Tzivion et al.*, 1987, 1989; *Feingold et al.*, 1988; *Reisin et al.*, 1996].

[12] Four hydrometeor species are considered: drops, ice crystals, graupel and snowflakes (aggregates). Each particle species is divided into 34 bins, with mass doubling for adjacent bins. The aerosol spectrum is represented by 43 bins.

[13] The warm microphysical processes include nucleation of drops, condensation and evaporation, collision-coalescence, and binary breakup. The cold processes are ice nucleation (deposition, condensation-freezing, contact nucleation, and immersion freezing), ice multiplication, deposition and sublimation of ice, ice-ice and ice-drop interactions, melting of ice particles, sedimentation of drops and ice particles.

[14] The aerosol module includes prognostic equations for the number concentration of aerosol particles and of the specific mass of aerosols in the air and in hydrometeors, and equations for impaction scavenging of aerosol particles by hydrometeors, aerosol regeneration following complete evaporation/sublimation of hydrometeors, gas-cloud interactions and aqueous phase oxidation of dissolved SO_2 by ozone and hydrogen peroxide.

[15] Some of the equations and formulae are presented here for reference in later discussions. The prognostic equation for the vertical velocity is

$$\frac{\partial w}{\partial t} = F_d(w) - D(w) - \frac{\partial \pi}{\partial z} - g\frac{\theta_v}{\theta_{v0}} - gM, \tag{1}$$

where F and D are the turbulent diffusion and advection operators; θ_v is the perturbation of virtual potential temperature; $\pi = \left(\frac{p}{P_0}\right)^{\frac{R}{Cp}}$ is the nondimensional pressure, where p is pressure, $P_0 = 1000$ hPa, R is the gas constant for dry air, and Cp is the specific heat capacity for a constant pressure process; θ_{v0} is the virtual potential temperature of the unperturbed atmosphere, g is the acceleration due to gravity; and M is the mixing ratio of water.

[16] The ice nucleation activation spectrum for deposition and condensation freezing nucleation is given by [*Meyers et al.*, 1992]

$$N_{id} = \exp(-0.639 + 0.1296S_i), \tag{2}$$

where N_{id} is the number of ice crystals per liter that can be nucleated at supersaturation S_i with respect to ice (in%).

[17] Parameterization of the number of ice crystals produced by contact nucleation due to thermophoresis, diffusiophoresis, and Brownian motion is formulated according to *Cotton et al.* [1986]. The number of aerosols available for contact nucleation at temperature T is given by

$$N_{ic} = \exp[-2.8 + 0.262(T_0 - T)] \tag{3}$$

following *Meyers et al.* [1992]. Here T_0 is set as 0°C.

[18] There are two types of parameterization of immersion freezing: the first type is the stochastic hypothesis, which assumes that the freezing results from a random formation of a critical size embryo and the presence of foreign particles increases the probability of ice nucleation without disturbing its stochastic nature [e.g., *Bigg*, 1953a]. The second type is the singular hypothesis, which assumes that the drop freezing temperature is determined by nuclei properties [e.g., *Vali*, 1994].

[19] For the first method, experimental studies have indicated that the freezing of supercooled drops is best simulated by a stochastic process and suggested that the probability of freezing depends on the volume of the drop and rate of cooling [e.g., *Bigg*, 1953b; *Gerber*, 1976; *DeMott and Rogers*, 1990; *Gorbunov et al.*, 2001]. *Bigg* [1953b] showed that for a drop of volume V cooled to a temperature T below 0°C for t seconds, the probability P that it will freeze is given by

$$\ln(1 - P) = -VtK[\exp(a(T_0 - T)) - 1], \tag{4}$$

where the factor $K[\exp(a(T_0 - T)) - 1]$ has been empirically determined and a and K are constants. *Bigg* [1953b] used $a = 0.82\ (°C)^{-1}$ and $K = 2.9 \times 10^{-8}$, while *Wisner et al.* [1972] chose $a = 0.66\ (°C)^{-1}$ and K might vary by as much as three orders of magnitude. Because a decrease in K by one order of magnitude is equivalent to a decrease in T of about 3.5°C, the variation of K would indicate a change in freezing characteristics on the order of 10°C for a same type of aerosols. *Pitter and Pruppacher* [1973] showed experimentally that the freezing rate followed algorithmically with drop volume only for temperatures below −15°C. The stochastic method of *Bigg* [1953b] has been used in many models [e.g., *Reisner et al.*, 1998; *Khain and Sednev*, 1996; *Reisin et al.*, 1996], including MAC3.

[20] In MAC3, the number of frozen drops per unit time depends on the number of drops, their mass, and the supercooling:

$$\frac{dN_f(m,t)}{dt} = N_w(m,t)\frac{m}{\rho_w}\bar{A}\exp[\bar{B}(T_0 - T)], \tag{5}$$

where N_f is the number of frozen drops with mass m. The parameters $\bar{A}$ and $\bar{B}$ are equal to 10^{-4} $cm^{-1}s^{-1}$ and $0.66\ K^{-1}$, respectively, as those used by *Orville and Kopp* [1977].

3. Experimental Design

[21] The model domain is 12 km in the vertical direction and 6 km in the radial direction. The vertical and horizontal resolutions are 300 m and 150 m, respectively. A time step of 2.5 s is used for condensation/evaporation of drops or deposition/sublimation of ice particles, and 0.01 for gas absorption. All other processes use a time step of 5 s.

[22] The initial conditions for the temperature and humidity fields use the profiles measured during the Cooperative Convective Precipitation Experiment (CCOPE) on 19 July 1981 in Miles City, Montana, USA. The profiles are shown in Figure 1a. Under moderately unstable stratification and relatively weak wind shear, an isolated deep convective cloud developed with limited precipitation.

[23] MAC3 is run here in as axisymmetric configuration, which is appropriate for the type of cloud that developed during the low wind shear conditions. In weak wind shear, an axisymmetric model gives more realistic results than a two-dimensional (2-D) slab-symmetric model for simulation of a single-cell cloud. For example, *Ogura* [1963], *Murry* [1970] and *Soong and Ogura* [1973] compared results from 2D slab-symmetric and axisymmetric models. All those studies showed that clouds that developed in an axisymmetric model were more vigorous than those in a 2D slab-symmetric model, and the clouds developed in an axisymmetric model were more close to those in a three dimensional model [*Wilhelmson and Ogura*, 1972], providing the initial and boundary conditions in the two models were the same [*Soong and Ogura*, 1973].

[24] The initial values of trace gases (CO_2, SO_2, H_2O_2, and O_3) on the surface level and their scale heights are listed in Table 3 of *Yin et al.* [2005]. For the simulations in this paper, the values for clean air are used. The size distribution of aerosol particles was fitted by superposing three lognor-

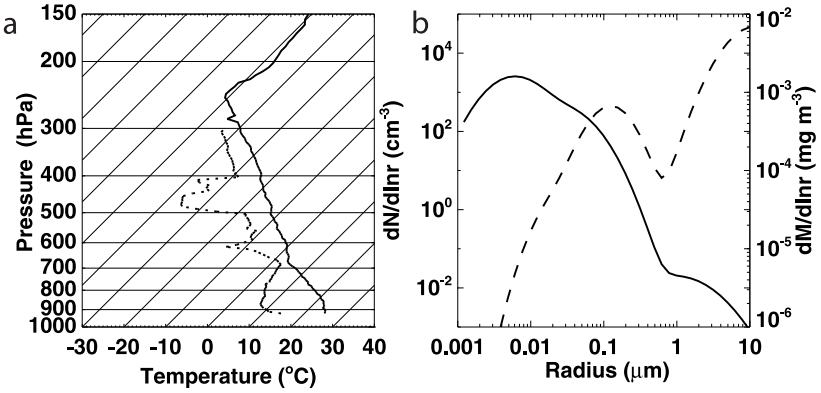

Figure 1. (a) Sounding of temperature (solid curve) and dew point temperature (dashed curve) for 1440 MDT, Miles City, Montana, United States, for 19 July 1981 and (b) initial number (solid curve) and mass (dashed curve) density distribution functions of aerosol particles (based on *Hobbs et al.* [1985] and *Respondek et al.* [1995]) used in the simulations.

mal distribution functions (Figure 1b) using the parameters given by *Respondek et al.* [1995]. The geometric mean aerosol particle radii of the three modes are 0.006, 0.03, and 1.0 μm, respectively. On the basis of *Hobbs et al.* [1985], *Yin et al.* [2005] assumed that 15% of the aerosol particles were water soluble, and that the soluble aerosols were composed of ammonium sulphate, regardless of size.

[25] The initial conditions for the aerosol size distribution and the resulting maximum droplet concentrations are given in Table 1. The three aerosol modes in Figure 1b are represented by m1, m2, and m3 referring to the Aitken, accumulation and coarse modes, respectively. In the simulations, only the amplitude of m2 was changed by 25%, 50%, 100% (the base case), 150% and 200%, and the codes of simulations are denoted, accordingly, as m2-25%, m2-50%, m2-100%, m2-150%, and m2-200%, respectively. The base case, m2-100%, is a reproduction of *Yin et al.* [2005] who found that the simulated cloud was in good agreement with the observations. The maximum droplet concentration (at cloud base) varies between about 650 in the m2-25% simulation and 1200 cm^{-3} in the m2-200% simulation and represents a realistic range for continental conditions.

4. Results

4.1. Temporal Variation

[26] Figure 2 shows the variations of maximum specific masses of the hydrometeors and the cloud top heights for the five cases in Table 1. In Figures 2a–2c, only the isopleths of specific mass being equal to 0.1 g kg^{-1} were plotted in order to clearly see how the vertical boundaries of the hydrometeors vary with time. Supercooled droplets reached about 8 km at around 30 min for all five cases (Figure 2a), with the top heights varying by only a few hundred meters. In contrast, the top heights of ice crystals and graupel were more divergent in the five simulations, decreasing as the aerosol concentrations were increased. For example, the top height of ice crystals and graupel in case m2-200% was almost 2 km lower than that in case m2-100% at 40 min. As a result, the overall cloud top heights were different: the higher the aerosol concentration, the lower the cloud top height during its mature stage (Figure 2d). Note also that in case m2-200%, the development of the cloud top height was strongly inhibited during 30–40 min.

[27] Figure 3 shows the temporal variations of the maximum vertical velocity, the maximum radar reflectivity factor, and the instantaneous rain rate. The maximum vertical velocities, w_{max}, were almost identical before 25 min and attained 15–16 m s^{-1} at about 25 min for all five cases. Between 25–55 min, w_{max} decreased as aerosol concentration increased. At 40 min, w_{max} was 9.8 m s^{-1} in the reference simulation m2-100%, while it was only 2.9 m s^{-1} in case m2-200%, a more than two-thirds reduction. Updrafts play a key role in convective clouds. It is in the updraft that water vapor condensates and droplets form. The stronger the updrafts, the longer the droplets are in the cloud before they fall as rain and the bigger they grow. The effects of aerosol concentration on the vertical velocity inevitably has a significant effect on cloud dynamics and microphysics. The axisymmetric model is appropriate for the type of cloud we are simulating, although it should be remembered that development of updrafts and downdrafts will be different in a sheared environment.

Table 1. Experimental Design of the Simulations[a]

Simulation Code	Size Distribution of Aerosol	Resulting Maximum Droplet Concentration, cm^{-3}
m2-100% (reference simulation)	Same as the reference simulation	930
m2-25%	Amplitude of mode 2 multiplied by 25%	873
m2-50%	Amplitude of mode 2 multiplied by 50%	920
m2-150%	Amplitude of mode 2 multiplied by 150%	1130
m2-200%	Amplitude of mode 2 multiplied by 200%	1235

[a]Here m2 stands for aerosol mode 2 and corresponds to the accumulation mode of the model aerosol size distribution.

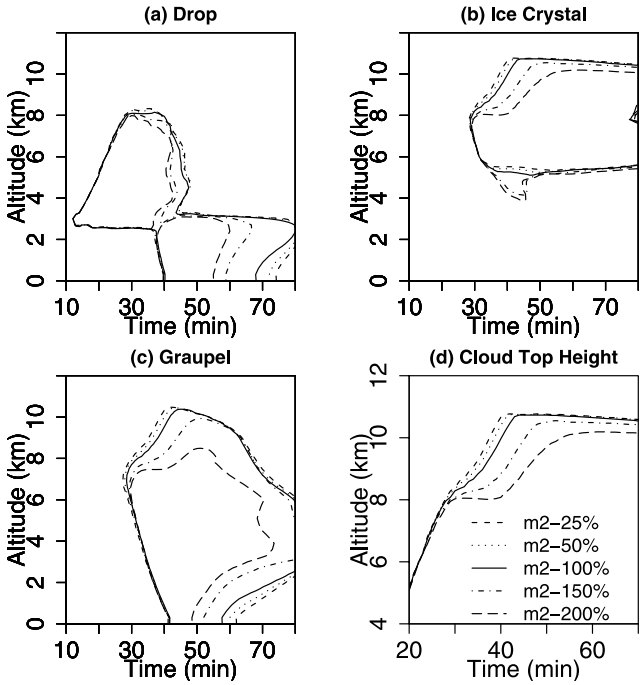

Figure 2. Temporal variation of the maximum specific mass for (a) droplet, (b) ice crystal, (c) graupel, and (d) simulated cloud top heights in cases m2-100%, m2-25%, m2-50%, m2-150%, and m2-200%. For clarity, only isopleth of 0.1 g kg^{-1} are plotted in Figures 2a–2c.

[28] Figure 3b shows a clear effect of aerosol concentration on the radar reflectivity factor: case m2-200% had the weakest radar echo, and case m2-25% the strongest. The higher the dBZ level, the more intense the precipitation.

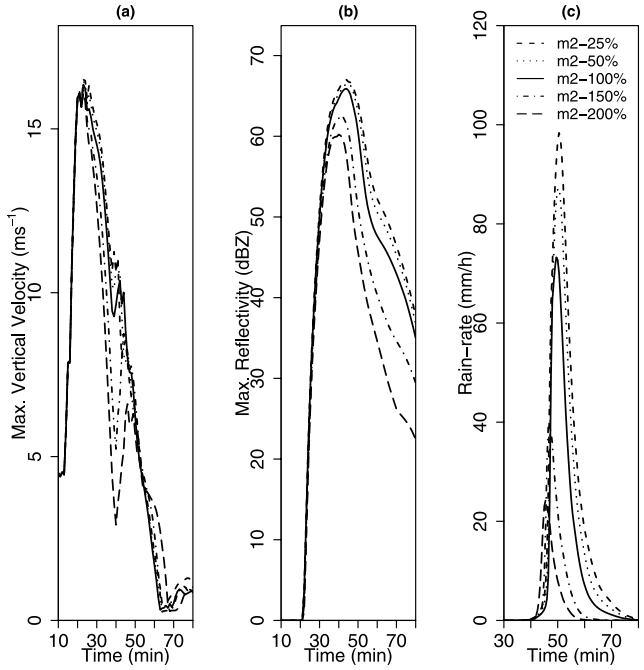

Figure 3. Temporal variation of the maximum of (a) vertical velocity, (b) radar reflectivity factor, and (c) instantaneous precipitation rate in cases m2-25%, m2-50%, m2-100%, m2-150%, and m2-200%.

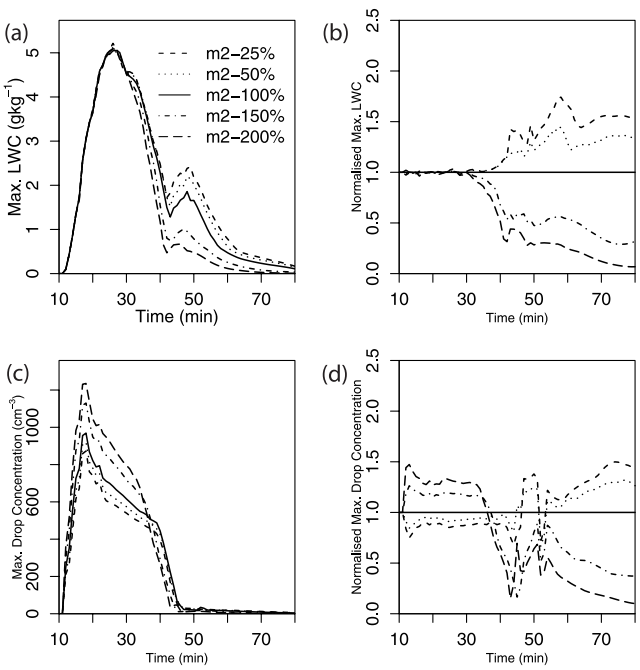

Figure 4. Temporal variation of the maximum values of (a) liquid water content (LWC), (b) LWC normalized to the reference simulation m2-100%, (c) number concentration of drops, and (d) number concentration of drops normalized to the reference simulation in cases m2-100%, m2-25%, m2-50%, m2-150%, and m2-200%.

Larger and more numerous hydrometeors in a unit volume produce larger Z_e. Conventionally, Z_e is converted into a logarithmic expression (dBZ), referenced to mm^6m^{-3}.) Least intense and shortest duration of precipitation in case m2-200% produced the lightest rain. Figure 3c shows the precipitation rate in the five cases. It can be seen that the peak rain rate in case m2-200% was only about 1/3 of that in case m2-100%. This result is consistent with previous research: increasing aerosols reduces precipitation efficiency [e.g., *Rosenfeld*, 2000; *Toon*, 2000; *Khain et al.*, 2004]. It is well known that favored conditions for precipitation are a wider range of droplet sizes, a deeper cloud thickness, and stronger updrafts within the clouds. Case m2-200%, least meeting these requirements therefore produced lightest rain. The possible reason for the earlier precipitation in the cases with more CCN was the increase in concentration of giant CCN when the concentration of mode 2 was increased.

[29] Figures 4, 5, and 6 show the time variation of the maximum values of water content and number concentration of the hydrometeors. For droplets before 35 min, the maximum liquid water contents (LWC) were very similar, but the number concentrations were very different. The maximum of number concentration was about 40% higher in case m2-200% than in case m2-100%. This means that smaller and more numerous droplets were produced when the aerosol concentrations were increased. The result is in line with previous findings for both convective and non-convective clouds [e.g., *Twomey*, 1977; *Coakley et al.*, 1987; *Albrecht*, 1989; *Radke et al.*, 1989; *King et al.*, 1993; *Ferek et al.*, 2000; *Rosenfeld*, 2000]. During 35–45 min, most supercooled droplets in all the clouds were either evaporated or fell as rain (see Figure 2a). After 45 min,

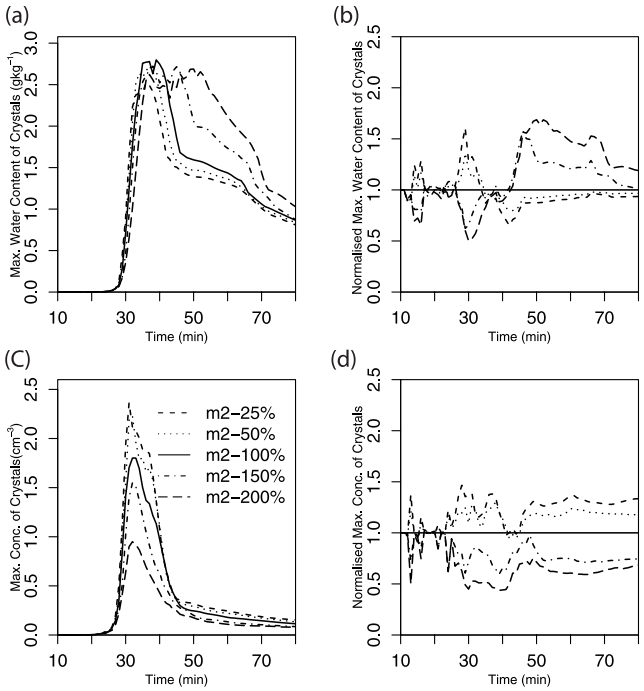

Figure 5. Same as Figure 4, but for ice crystals.

both the maximum LWCs and number concentrations decreased as the aerosol concentrations were increased. Note the fact that they were falling drops; therefore raindrops on average were smallest in case m2-200%.

[30] The maximum number concentration of ice crystals decreased with increased aerosol concentrations, being about 50% lower in case m2-200% than in m2-100%. The crystal specific mass behaved differently before and after 40 min (Figure 5). Before 40 min, the maximum specific mass decreased as the aerosol concentration increased but the situation reversed after 40 min. Table 2 shows maximum rates of various ice formation processes in two cases (the base case and m2-200%) at selected times. In the two cases, the vapor deposition and condensation freezing dominated the ice formation before 30 min; between 30 and 40 min, immersion freezing of drops became the most important processes. The high production rate of ice crystals before 30 min was related to the high supersaturation with respect to ice, and this is consistent with the previous study of *Yin et al.* [2002]. During 30–40 min, the rates due to immersion freezing and deposition/condensation freezing were about 2–3 times higher in case m2-100% than those in case m2-200%. There are two reasons for the higher rates: first, the supersaturation with respect to ice was higher and this resulted in a higher rate of deposition/condensation freezing (see Figures 7 and 8); secondly, the drops were more numerous and larger near the top of the m2-100% cloud than in the m2-200% cloud (see Figure 9) and this produced more ice crystals by immersion freezing, as is suggested by equation (5). After 40 min, immersion freezing was no longer the dominant process for ice production because drops had been consumed by riming. However, deposition and condensation freezing became dominant because sufficient water vapor in the updraft provided a supersaturated environment for ice production.

[31] For graupel in Figure 6, a decrease in the maximum water concentration is apparent as the aerosol concentration increased. The values are about 20–30% higher in cases m2-25% and m2-50% than those in case m2-100%. In cases m2-150% and m2-200%, they were more than 50% lower in the later stage of the simulation. The maximum number concentration of graupel was lower as the aerosol concentration increased before 40 min. The formation of graupel was due mainly to freezing of large drops (diameter larger than 100 μm in this study) and to coagulation between drops and ice particles. Those two processes were more vigorous in cases m2-100% than in case m2-200% (see Table 2). Between 40–60 min, case m2-150% and m2-200% had slightly higher number concentration than the base case.

4.2. Dynamical Analysis

[32] Figures 2–6 indicate that cloud dynamics and microphysics were sensitive to initial aerosol concentrations after 30 min, especially for case m2-200% with a stagnant cloud top for about 10 min. The stagnation was related to a halt of updraft at the cloud top level. Because updrafts in a convective cloud are driven primarily by buoyancy and affected by other forces (equation (1)), a momentum budget of the equation for the vertical velocity is useful in determining the effects of microphysical processes on the cloud dynamics. In this section we examine the latent heat changes associated with ice formation and droplet evaporation in order to understand how the temperature perturbation at cloud top as well as the vertical velocity distribution differed in cases m2-100% and m2-200%. Then, we examine the differences in the momentum budgets for the two cases in order to understand how changes in the two dominant forces (buoyancy and water loading) are related to microphysical changes at cloud top.

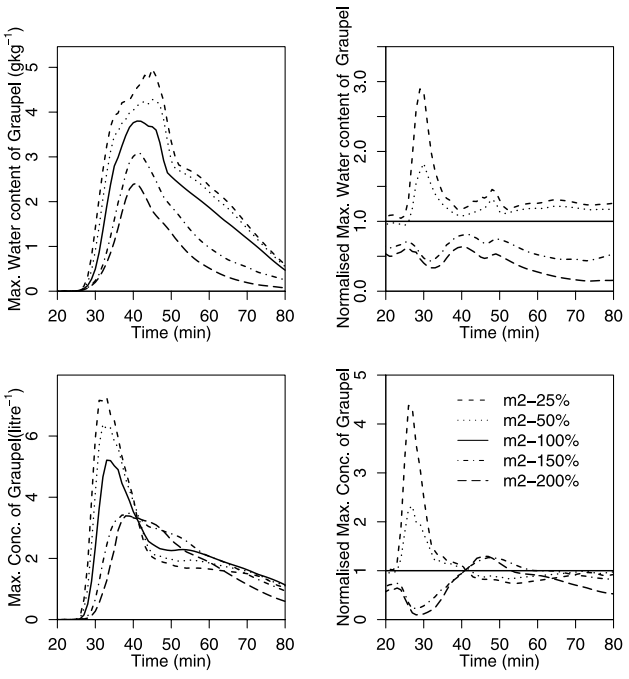

Figure 6. Same as Figure 4, but for graupel.

Table 2. Maximum Rate for Ice Formation Via Various Microphysical Processes at Selected Times in Cases m2-100% and m2-200%[a]

	20 min	25 min	30 min	35 min	40 min	45 min	50 min	55 min	60 min	65 min	70 min
Imfr											
m2-100%	–	173.9	17580.0	6196.0	3043.0	7.1	–	–	–	–	–
m2-200%	–	140.9	7672.0	1421.0	75.5	2.7	–	–	–	–	–
Depo											
m2-100%	62.0	1260.0	567.4	645.8	608.6	507.2	377.5	252.4	–	–	–
m2-200%	85.6	1407.0	307.9	141.2	34.8	41.7	358.0	313.5	108.3	–	–
Cont	–	–	–	–	–	–	–	–	–	–	–
Mult											
m2-100%	–	–	–	22.7	60.6	5.7	–	–	–	–	–
m2-200%	–	–	–	19.6	14.6	–	–	–	–	–	–
Gcol											
m2-100%	–	–	2.7	9.6	10.9	–	–	–	–	–	–
m2-200%	–	–	1.9	15.4	3.2	–	–	–	–	–	–

[a]Units are m^{-3} s^{-1}. Imfr, immersion freezing; Depo, deposition and condensation freezing; Cont, contact freezing; Mult, ice multiplication; Gcol, production of graupel by coagulation of ice particles and drops. Values smaller than 10^0 are not shown.

[33] Figures 7 and 8 show the saturation ratios with respect to water and with respect to ice, together with the outlines of droplets and ice crystals for cases m2-100% and m2-200%. In the area bounded by the dotted and dashed curves, the air contained droplets but was unsaturated with respect to water. Therefore the droplets evaporated. However, it was supersaturated with respect to ice so the ice crystals grew at the expense of the droplets. This process is known as the Wegener-Bergeron-Findeisen mechanism [*Wegener*, 1911; *Bergeron*, 1935; *Findeisen*, 1938]. The rate of release of latent heat under these conditions is determined by the rate of conversion of water mass into ice mass. In these clouds with different aerosol it is the immersion freezing rate that dominates the rate of formation of ice at cloud top. Figure 9 shows the difference in vertical velocity (Δw), the difference in number concentration of drops (ΔN_d), and the difference in LWC of drops (ΔM_d) between cases m2-100% and m2-200% at 20, 25, 30, and 35 min. Generally, the updrafts were stronger and the number concentration of drops was less in case m2-100%, but the trend was reversed in a thin layer near cloud top: there are more drops and a higher LWC in the m2-100% cloud at 25, 30, and 35 min. The *Bigg* [1953b] formula, as discussed in section 2, shows that the probability of drop freezing increases exponentially with drop volume. The parameterization of immersion freezing based on the Bigg scheme in MAC3 therefore produced more ice crystals, more ice mass, and a more rapid release of latent heat than in case m2-100% than in m2-200% in the top part of the cloud.

[34] The heating, (i.e., $\Delta T > 0$, where $\Delta T = T_{35\text{min}} - T_{0\text{min}}$) was weaker in intensity and narrower in spatial extent within 1.5 km from the cloud centers in case m2-200% than that in case m2-100% (Figure 10). In case m2-100% the maximum heating was 2.5°C (Figure 10a), but in case m2-200% it was only about 1°C (Figure 11a). A maximum of 1.5°C of heating was located just above 8 km near the cloud top in case m2-100% (Figure 10a). In contrast, a maximum of 0.5°C heating was below 8 km in case m2-200% (Figure 11a). The cooling between 2–6 km around the edge of the cloud was stronger in case m2-200% than that in case m2-100%, especially near the cloud tops. The small droplets have a larger total surface area than the same amount of liquid in a big droplet. This allows small droplets to evaporate quickly, as was in case m2-200%.

[35] The vertical velocity fields of the two cases were similar in structure: an updraft core was surrounded by downdrafts (Figure 11b). This is consistent with the observations by *Kollias et al.* [2001] using radar observations. However, they were fairly different in intensity: updrafts were stronger, wider, and deeper in case m2-100% (Figure 10b) than those in case m2-200% (Figure 11b). The downdrafts which flanked the core updraft were stronger in case m2-200%. There were several local minima in the vertical velocity field in case m2-200%. A weaker one

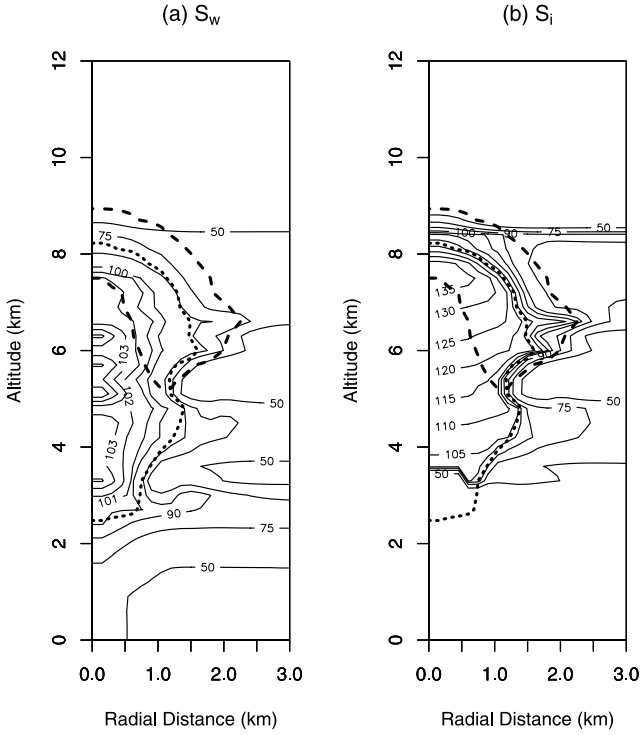

Figure 7. Saturation ratios (solid curves) with respect to water (S_w) and with respect to ice (S_i) as well as the outlines of droplets (dotted curve) and ice crystals (dashed curves) in the radial cross section at 35 min in case m2-100% (solid curves). For droplets and ice crystals, the outlines are plotted for the isopleth of 0.1 g kg^{-1}.

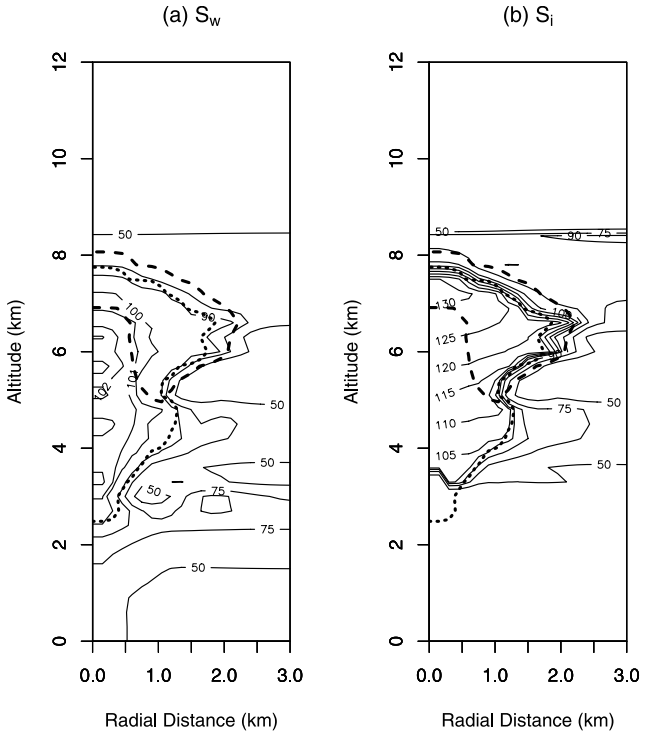

Figure 8. Same as Figure 7, but for case m2-200%.

located at about 3 km, which was around the freezing level, seems to be related to melting and evaporation. The other minimum between 4–6 km is associated with a dry layer at that level. Together, those downdrafts almost reached the ground and therefore substantially cut off the supply of inflow air in the boundary layer. Insufficient inflow in the boundary layer and less heating near the cloud top combine to diminish the development of the cloud in case m2-200% (Figure 2d) during 30–40 min. An important impact of wind shear is to separate downdrafts from updrafts in a storm. If the ambient wind shear is very weak, as here, axisymmetry is a good approximation. If there is no wind shear, downdrafts can destroy the updraft during the dissipating stage of a single-cell storm. If wind shear exists, the separation of downdraft from updraft affects the dynamic organization and persistence of a storm.

[36] Finally, Figure 12 shows the momentum budget at 35 min for cases m2-100% and m2-200%. The five terms from left to right in equation (1) are denoted as tend, diff, adv, pg, buoy, load, respectively, in Figure 12. It can be seen that the local accelerations are very different: in case m2-100%, vertical velocities were accelerated between 7 and 9 km with a deep layer of weak deceleration underneath; while in case m2-200%, the local accelerations were close to zero between 7.5 and 9 km with a deep layer of strong deceleration underneath. The two biggest forces near the cloud tops were buoyancy and water loading. In case m2-100%, the buoyancy force outweighed water loading, and the result was acceleration, while in case m2-200% the two forces were equally important and cancelled each other out, and the result was very weak acceleration. The strong acceleration near the cloud top in case m2-100% indicated that the cloud in this case continually grew. In contrast, in case m2-200%, the cloud development stalled.

5. Comparison With Previous Studies

[37] Our results differ from previous numerical studies of cloud response to changing aerosol [e.g. *Khain et al.*, 1999; *Khain and Pokrovsky*, 2004]. In particular, increased aerosol concentrations in our simulations led to a less deep, less vigorous cloud with fewer (but larger) ice crystals in the anvil. The previous study most similar to ours is that of *Khain et al.* [2004] of a cloud in Texas under fairly dry continental conditions. They found that increased aerosol concentrations resulted in a more vigorous and deeper cloud with a higher concentration of ice crystals in the anvil, opposite to what we have found. Both studies simulated a decrease in precipitation with increased aerosol.

[38] The different responses can be explained by two major differences between the two clouds and the setup of the experiments. The CCOPE cloud over Montana studied here existed predominantly below the homogeneous freezing level so ice formation was dominated by heterogeneous freezing mechanisms. The Texas cloud studied by *Khain et al.* [2004] ascended to 14 km and ice formation was dominated by homogeneous freezing. The second difference between the two experiments is that we studied a realistic range of continental aerosol concentrations, while *Khain et al.* [2004] show results for continental and maritime-type aerosol conditions but applied in both cases to a cloud forming in a continental environment. Thus, in the Khain et al. study, a significant difference between their high- and low-aerosol cases (continental and maritime) was the amount of rain produced through warm microphysical processes of drop collision and coalescence. "Warm rain" production in the low-aerosol (maritime) case significantly reduced the number of drops ascending above the homogeneous freezing level and therefore directly reduced the number of crystals in the anvil and also reduced the latent heat release there. Rain formation in the low-aerosol case also increased the loading and further suppressed the updrafts. Warm rain was not effective in any of our continental simulations. Ice production was dominated by heterogeneous immersion freezing, which was faster in the low-aerosol case with larger droplets, resulting in more crystals in the anvil, a greater latent heat release, and hence greater vertical development in the mature stage.

6. Conclusions and Future Work

[39] In this paper we have studied the response of cloud dynamics and microphysics to aerosol concentrations using an axisymmetric nonhydrostatic numerical model of a convective cloud with detailed treatment of microphysical processes and atmospheric aerosols. The model was initialized with observed meteorological conditions on 19 July 1981 near Miles City, Montana, USA during the Cooperative Convective Precipitation Experiment (CCOPE). Under this continental environment, a deep mixed-phase convective cloud developed with moderate precipitation. The results of *Yin et al.* [2005] showed that the model reproduced reasonably well the macrostructure and microstructure of the observed cloud. In the work by *Yin et al.* [2005],

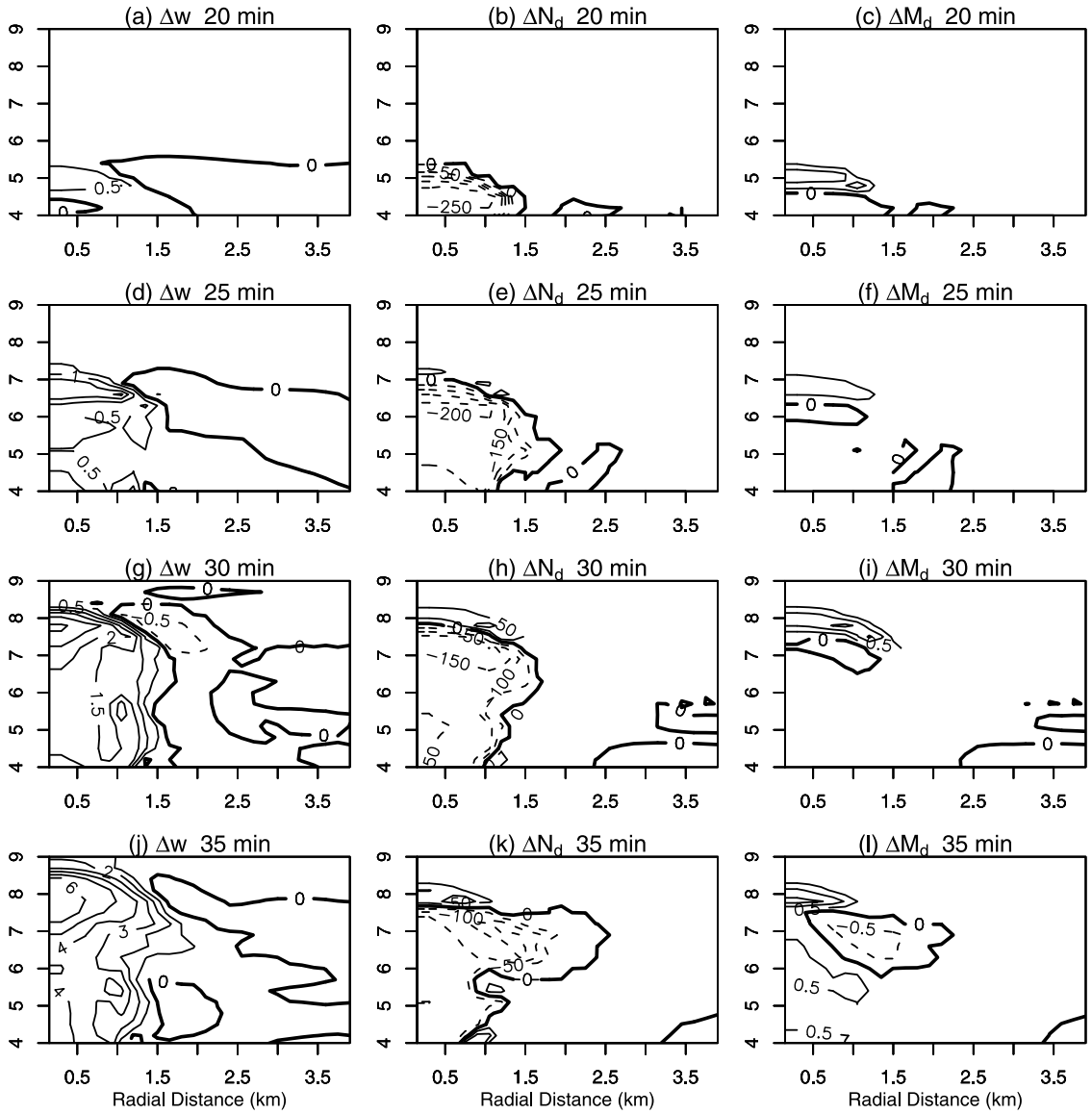

Figure 9. Difference in vertical velocity (Δw, m s^{-1}), the difference in number concentration of drops (ΔN_d, cm^{-3}), and the difference in LWC of drops (ΔM_d, g kg^{-1}) between cases m2-100% and m2-200% at 20, 25, 30, and 35 min.

the aerosol distribution was fitted by superimposing three lognormal distribution functions. In this study, we investigated the response of the dynamics and microphysics of the simulated cloud to aerosol concentration by varying the amplitude of aerosol mode 2 (the accumulation mode).

[40] As the aerosol concentrations increased, there were more numerous and smaller drops in the clouds. As the clouds developed and their tops reached the midtroposphere and above, the dry continental atmosphere provided insufficient water vapor supply. The air was subsaturated with respect to water within a layer of several hundred meters thick near cloud top although it was supersaturated with respect to ice. Near the cloud tops, immersion freezing was the main process determining cloud development. The drops were smaller and less numerous near cloud top in cases with higher aerosol concentrations, a tendency explained by the more rapid evaporation of smaller drops in the dry continental air. Therefore immersion freezing was less vigorous near the tops of clouds with high aerosol concentrations. This process reduced the buoyancy at cloud top and produced stronger downdrafts flanking the updraft core of the high-aerosol clouds. As a result, the cloud developed slower. For the case in which the number of particles in mode 2 (the accumulation mode) was doubled, we found that (1) the cloud development even stagnated during 30–40 min; (2) the top of graupel reached only 8 km, 2 km lower than that in the base case; (3) the inflow within the boundary layer was cut off; (4) the updraft was weaker and the downdraft stronger; and (5) the precipitation was suppressed by about two thirds.

[41] A comparison of our results with several previous studies indicates that aerosol affects cloud dynamics, mi-

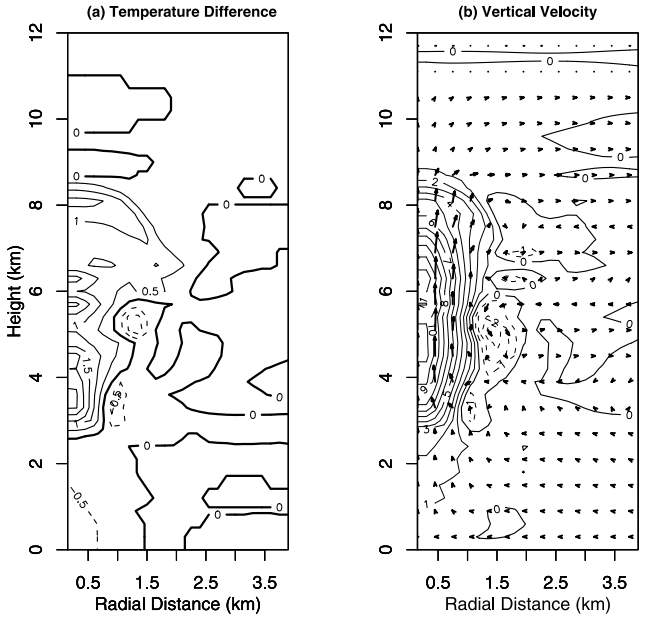

Figure 10. (a) Radial cross section of temperature changes at 35 min from their initial values and (b) radial cross section of vertical velocity at 35 min together with wind arrows in case m2-100%.

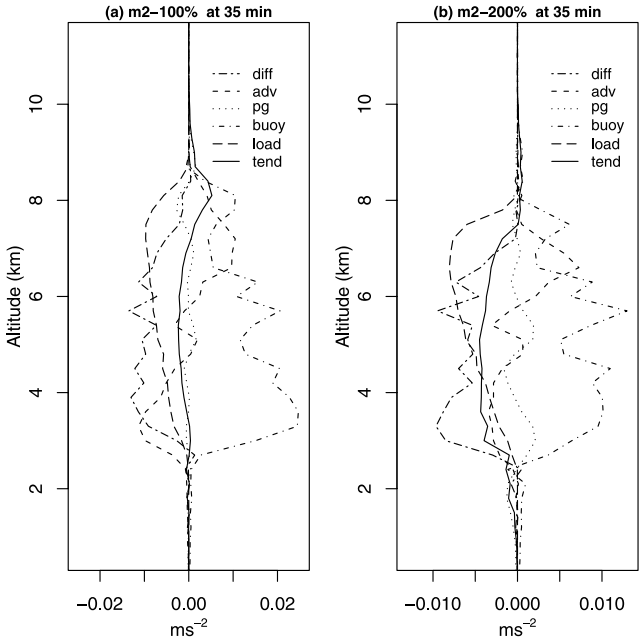

Figure 12. Momentum budget of vertical velocity for cases m2-100% and m2-200% at 35 min. See text for details.

crophysics, and thermodynamics in different ways depending on the height of the cloud, the efficiency of warm rain production, and the mechanisms responsible for ice formation. In general, the microphysical and dynamical properties of the simulated cloud agree very well with extensive observations [*Yin et al.*, 2005], giving us confidence that the treatments of microphysical processes in the model are reasonably realistic. However, the ice formation mechanisms responsible for driving the response to aerosol in these simulations are uncertain. Further studies of mixed phase clouds below the homogeneous freezing level are needed to determine the importance of uncertainties in ice microphysics in attempts to quantify cloud response to aerosols. Further studies should also examine whether the cloud responses in the low vertical wind shear environment also occur under conditions of high wind shear.

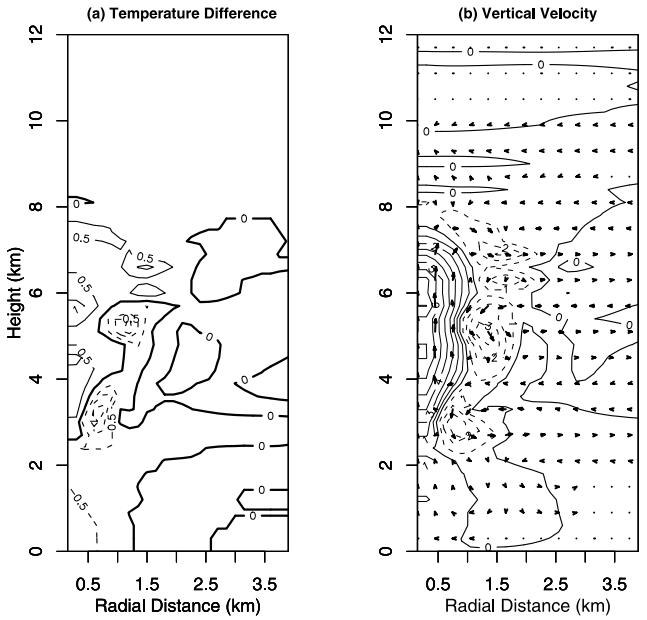

Figure 11. Same as Figure 10, but in case m2-200%.

[42] **Acknowledgment.** The project was partly funded by two EU projects (PARTS: Particles in the Upper Troposphere and Their Influence on Climate and TROCCINOX: The Tropical Convection and Nitrogen Oxides Experiment) and by a UK Natural Environment Research Council grant Modeling the Modification of Convective Clouds due to Anthropogenic Aerosol (MMOCCAA), grant NE/B50469X/1.

References

Albrecht, B. A. (1989), Aerosol, cloud microphysics, and fractional cloudiness, *Science*, *245*, 1227–1230.

Andreae, M. O., D. Rosenfeld, P. Artaxo, A. A. Costa, G. P. Frank, K. M. Longo, and M. A. F. Silva-Dias (2003), Smoking rain clouds over the Amazon, *Science*, *303*, 1337–1342.

Bergeron, T. (1935), On the physics of clouds and precipitation, paper presented at 5th IUGG Assembly, Int. Union of Geod. and Geophys., Lisbon.

Bigg, E. K. (1953a), The supercooling of water, *Proc. Phys. Soc. London*, *66*, 688–694.

Bigg, E. K. (1953b), The formation of atmospheric ice crystals by the freezing of droplets, *Q. J. R. Meteorol. Soc.*, *79*, 510–519.

Charlson, R. J., S. E. Schwartz, J. M. Hales, R. D. Cess, J. A. Coakley Jr., J. E. Hansen, and D. J. Hoffman (1992), Climate forcing by anthropogenic aerosols, *Science*, *255*, 423–430.

Coakley, J. A., Jr., R. L. Bernstein, and P. A. Durkee (1987), Effect of shipstack effluents on cloud reflectivity, *Science*, *237*, 1020–1022.

Cotton, W. R., G. J. Tripoli, R. M. Rauber, and E. Mulvihill (1986), Numerical simulation of the effects of varying ice crystal nucleation rates and aggregation processes on orographic snowfall, *J. Clim. Appl. Meteorol.*, *25*, 1658–1680.

DeMott, P. J., and D. C. Rogers (1990), Freezing nucleation rates of dilute solution droplets measured between −30 and −40°C in laboratory simulations of natural clouds, *J. Atmos. Sci.*, *47*, 1056–1064.

Ekman, A. M. L., C. Wang, J. Wilson, and J. Ström (2004), Explicit simulations of aerosol physics in a cloud-resolving model: A sensitivity

study based on an observed convective cloud, *Atmos. Chem. Phys.*, *4*, 773–791.
Feingold, G., S. Tzivion, and Z. Levin (1988), The evolution of raindrop spectra: Part I. Stochastic collection and breakup, *J. Atmos. Sci.*, *45*, 3387–3399.
Ferek, R. J., et al. (2000), Drizzle suppression in ship tracks, *J. Atmos. Sci.*, *57*, 2707–2728.
Findeisen, W. (1938), Die kolloidmeteorologischen Vorgänge bei der Niederschlagsbildung, *Meteorol. Z.*, *55*, 121–133.
Fridlind, A. M., et al. (2004), Evidence for the predominance of mid-tropospheric aerosols as subtropical anvil cloud nuclei, *Science*, *304*, 718–722.
Gerber, H. E. (1976), Relationship of size and activity for AgI smoke particles, *J. Atmos. Sci.*, *33*, 667–677.
Gorbunov, B., A. Baklanov, N. Kakutkina, H. L. Windsor, and R. Toumi (2001), Ice nucleation on soot particles, *J. Aerosol Sci.*, *32*, 199–215.
Graf, H.-F. (2004), The complex interaction of aerosols and clouds, *Science*, *203*, 1309–1311.
Hobbs, P. V., D. A. Bowdle, and L. F. Radke (1985), Particles in the lower troposphere over the high plains of the United States: Part I. Size distributions, elemental composition and morphologies, *J. Clim. Appl. Meteorol.*, *24*, 1344–1356.
Intergovernmental Panel on Climate Change (IPCC) (2001), *Climate Change 2001: The Scientific Basis: Summary for Policymakers and Technical Summary of the Working Group I Report*, 20 pp., edited by J. T. Houghton et al., Cambridge Univ. Press, New York.
Khain, A., and A. Pokrovsky (2004), A simulation of effects of atmospheric aerosols on deep turbulent convective clouds using a spectral microphysics mixed-phase cumulus cloud model. part II: Sensitivity study, *J. Atmos. Sci.*, *61*, 2983–3001.
Khain, A. P., and I. Sednev (1996), Simulation of precipitation formation in the eastern Mediterranean coastal zone using a spectral microphysics cloud ensemble model, *Atmos. Res.*, *43*, 77–110.
Khain, A. P., A. Pokrovsky, and I. Sednev (1999), Some effects of cloud-aerosol interaction on cloud microphysics structure and precipitation formation: Numerical experiments with a spectral microphysics cloud ensemble model, *Atmos. Res.*, *52*, 195–220.
Khain, A., A. Pokrovsky, M. Pinsky, A. Seifert, and V. T. J. Phillips (2004), Simulation of effects of atmospheric aerosols on deep turbulent convective clouds by using a spectral microphysics mixed-phase cumulus cloud model. part 1: Model description and possible applications, *J. Atmos. Sci.*, *61*, 2963–2982.
King, M. D., L. F. Radke, and P. V. Hobbs (1993), Optical properties of marine stratocumulus clouds modified by ships, *J. Geophys. Res.*, *98*, 2729–2739.
Kollias, P., B. A. Albrecht, R. Lhermitte, and A. Savtchenko (2001), Radar observations of updrafts, downdrafts, and turbulence in fair-weather cumuli, *J. Atmos. Sci.*, *58*, 1750–1766.
Meyers, M. P., P. J. DeMott, and W. R. Cotton (1992), New primary ice-nucleation parameterizations in an explicit cloud model, *J. Appl. Meteorol.*, *31*, 708–721.
Murry, F. W. (1970), Numerical models of a tropical cumulus cloud with bilateral and axial symmetry, *Mon. Weather Rev.*, *98*, 14–28.
Ogura, Y. (1963), The evolution of a moist convective element in a shallow, conditionally unstable atmosphere: A numerical calculation, *J. Atmos. Sci.*, *20*, 407–424.
Orville, H. D., and F. J. Kopp (1977), Numerical simulation of the life history of a hailstorm, *J. Atmos. Sci.*, *34*, 1596–1618.
Phillips, V. T. J., T. W. Choularton, A. M. Blyth, and J. Latham (2002), The influence of aerosol concentrations on the glaciation and precipitation of a cumulus cloud, *Q. J. R. Meteorol. Soc.*, *128*, 951–971.
Pitter, R. L., and H. R. Pruppacher (1973), A wind tunnel investigation of freezing of small water drops falling at terminal velocity in air, *Q. J. R. Meteorol. Soc.*, *99*, 540–550.
Radke, L. F., J. A. Coakley Jr., and M. D. King (1989), Direct and remote sensing observations of the effects of ships on clouds, *Science*, *246*, 1146–1149.
Ramanathan, V., and A. M. Vogelmann (1997), Greenhouse effect, atmospheric solar absorption and the Earth's radiation budget: From the Arrhenius-Langley era to the 1999s, in *The Legacy of Svante Arrhenius: Understanding the Greenhouse Effect*, edited by H. Rodhe and R. Charlson, pp. 85–103, R. Swed. Acad. of Sci., Stockholm Univ., Stockholm.
Ramanathan, V., P. J. Crutzen, J. T. Kiehl, and D. Rosenfeld (2001), Aerosols, climate, and the hydrological cycle, *Science*, *294*, 2119–2124.
Reisin, T., Z. Levin, and S. Tzivion (1996), Rain production in convective clouds as simulated in as axisymmetric model with detailed microphysics. part II: Effects of varying drops and ice initiation, *J. Atmos. Sci.*, *53*, 1815–1837.
Reisner, J., R. M. Rasmussen, and R. Bruintjes (1998), Explicit forecasting of supercooled liquid water in winter storms using the MM5 model, *Q. J. R. Meteorol. Soc.*, *124*, 1071–1107.
Respondek, P. S., R. R. Alheit, and H. R. Pruppacher (1995), A theoretical study of the wet removal of atmospheric pollutants, V. The uptake, redistribution, and deposition of $(NH_4)_2SO_4$ by a convective cloud containing ice, *J. Atmos. Sci.*, *52*, 2121–2132.
Rosenfeld, D. (2000), Suppression of rain and snow by urban and industrial air pollution, *Science*, *287*, 1793–1796.
Rosenfeld, D., and W. L. Woodley (2000), Convective clouds with sustained highly supercooled liquid water down to −37.5°C, *Nature*, *405*, 440–442.
Soong, S.-T., and Y. Ogura (1973), A comparison between axisymmetric and slab-symmetric cumulus cloud models, *J. Atmos. Sci.*, *30*, 879–893.
Toon, O. B. (2000), How pollution suppresses rain, *Science*, *287*, 1763–1765.
Twomey, S. (1977), *Atmospheric Aerosols*, 302 pp., Elsevier, New York.
Twomey, S. (1991), Aerosols, clouds and radiation, *Atmos. Environ., Part A*, *25*, 2435–2442.
Tzivion, S., G. Feingold, and Z. Levin (1987), An efficient numerical solution to the stochastic collection equation, *J. Atmos. Sci.*, *44*, 3139–3149.
Tzivion, S., G. Feingold, and Z. Levin (1989), The evolution of raindrop spectra: Part II. Collisional collection/breakup and evaporation in a rainshaft, *J. Atmos. Sci.*, *46*, 3312–3327.
Vali, G. (1994), Freezing rate due to heterogeneous nucleation, *J. Atmos. Sci.*, *51*, 1843–1856.
Wegener, A. (1911), *Thermodynamik der Atmosphäre*, Barth, Leipzig, Poland.
Wilhelmson, R., and Y. Ogura (1972), The pressure perturbation and the numerical modeling of a cloud, *J. Atmos. Sci.*, *29*, 1295–1307.
Wisner, C., H. D. Orville, and C. Myers (1972), A numerical model of a hail-bearing cloud, *J. Atmos. Sci.*, *29*, 1160–1181.
Yin, Y., Z. Levin, T. Reisin, and S. Tzivion (2000), The effects of giant cloud condensation nuclei on the development of precipitation in convective clouds—A numerical study, *Atmos. Res.*, *53*, 91–116.
Yin, Y., K. S. Carslaw, and D. J. Parker (2002), Redistribution of trace gases by convective clouds–mixed-phase processes, *Atmos. Chem. Phys.*, *2*, 293–306.
Yin, Y., K. S. Carslaw, and G. Feingold (2005), Vertical transport and processing of aerosols in a mixed-phase convective cloud and the feedback on cloud development, *Q. J. R. Meteorol. Soc.*, *131*, 221–246.

K. S. Carslaw, Z. Cui, and S. Davies, Institute for Atmospheric Science, School of Earth and Environment, University of Leeds, Leeds LS2 9JT, UK. (zhiqiang@env.leeds.ac.uk)

Y. Yin, Department of Applied Meteorology, Nanjing University of Information Science and Technology, 114 Panchengxin Street, Pukou, Nanjing 210044, China.